scientific reports

Check for updates

OPEN

Linear and nonlinear thermoelectric transport in a quantum spin Hall insulators coupled with a nanomagnet

Rui Wang✉, Hui Liao, Chun-Yan Song, Guang-Hui Tang & Ning-Xuan Yang

Thermoelectric effects in quantum systems have been focused in recent years. Thermoelectric energy conversion study of systems with edge states, such as quantum Hall insulators and quantum spin Hall insulators, is one of the most important frontier topics in material science and condensed-matter physics. Based on the previous paper (Gresta in Phys Rev Lett 123:186801, 2019), we further investigated the linear and nonlinear thermoelectric transport properties of helical edge states of the quantum spin Hall insulators coupled with double nanomagnet, calculated the Seebeck coefficients S_c and the thermoelectrical figure of merit ZT, discussed the influence of the length of the nanomagnet and the relative tilt angle of component of the magnetization perpendicular on the thermoelectric coefficients (S_c and ZT), and summarized some meaningful conclusions in the linear response regime. In the nonlinear regime, we calculated the equivalent figure of merit ZT_M and the power-generation efficiency η in different length of the nanomagnet, obtain the temperature difference of achieving optimal thermoelectricity. The results of this paper further confirm that the setup can indeed be used as a device for achieving high performance thermoelectric.

Heat energy and electric energy are common forms of energy in the nature. Turning the waste heat into usable electric energy can not only alleviate the energy crisis, but also reduce environmental pollution[1,2]. It was early discovered that thermoelectric effect enables the interconversion between heat and electric energy[1–8]. Thermoelectric effects include the Seebeck effect, the Peltier effect, and the Thomson effect. Among these, the Seebeck effect is the thermalgradient-induced bias in a two-probe system, which describes a longitudinal thermoelectric effect[6,7,9–12]. Based on the thermoelectric effect, the thermoelectric energy conversion technology was developed to achieve thermoelectric power generation or thermoelectric refrigeration. Manufactured thermoelectric-devices can be widely used in industrial, space probes, military and medical equipment, and so on[1,13,14].

To achieve applicable thermoelectric-setup, it requires efficient thermoelectric conversion materials. The conversion efficiency of thermoelectric material depends on its thermoelectric figure of merit ZT. ZT is defined as $ZT = GS_c{}^2\mathcal{T}/\kappa$ (G is the electric conductance, S_c is the Seebeck coefficient, κ is the thermal conductance, and $\mathcal{T}$ is the absolute temperature of the device)[12,14–17]. The larger S_c and G, the smaller κ, the higher ZT value of the thermoelectric material, the better its performance. However, due to the restriction of the Mott relation and the Wiedemann–Franz law[3,18], S_c, G and κ are interrelated and cannot be regulated alone. In general, the increase of the charge carriers improved the electric conductance G , but it also causes the decrease of the Seebeck coefficient S_c and the increase of the thermal conductance κ, that is to say, any parameter will produce the corresponding parameter offset effect, so that the increase of ZT is not obvious[1–3]. Therefore, it is necessary to get the optimal ZT from the global perspective.

Most of the previous work of thermoelectric transport in nanoscale systems focused on the linear response mechanism of electric and thermal current to the electric potential or temperature difference, and the linear response theory and Onsager symmetry relations are used to obtain linear response coefficients such as electric conductance, thermal conductance and thermal power S_c. However, in the linear regime, since the temperature difference $\delta\mathcal{T}$ is much smaller than the temperature ($\delta\mathcal{T} \ll \mathcal{T}$), the efficiency η remains very low even if thermoelectric figure of merit ZT can be very large, $\eta \approx \delta\mathcal{T}/\mathcal{T} \ll 1$[19–21]. Nonlinear effects in nanoscale systems require the application of large driving forces at small distances, and nonlinearity has been predicted to cause thermal rectification effects[22,23] and low temperature cooling[24]. A deep understanding of nonlinear effects is needed to

Department of Physics, College of Sciences, Shihezi University, Shihezi 832000, China. ✉email: wr_tea@shzu.edu.cn

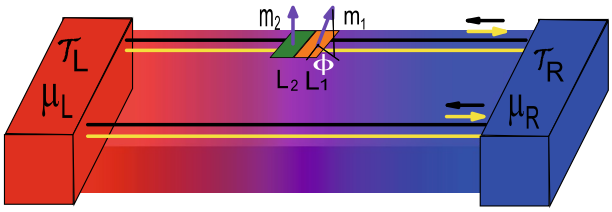

Figure 1. Schematic diagram of a QSHI system connected to a hot and a cold lead. Two nanomagnets with magnetic moments m_1 and m_2 and lengths L_1 and L_2 are contacted to a helical Kramers pair of edge states. A thermal gradient $\Delta\mathcal{T} = \mathcal{T}_L - \mathcal{T}_R$ is applied. We consider $\Delta\mathcal{T} = \mathcal{T}_L - \mathcal{T}_R > 0$ and $\Delta\mu = \mu_L - \mu_R$ and set $\mathcal{T} = \mathcal{T}_R$.

evaluate the thermal performance of thermal engines and multi-terminal thermal-electric conversion devices. Therefore, it is important to investigate the nonlinear thermoelectric properties of the nanosystems[19–21].

Topological insulator is a topological material newly discovered in recent years. It has an insulating body state and a conductive metallic surface state. The surface state is protected by the time-reversal symmetry of nonmagnetic impurity scattering[25,26]. Many studies have shown that topological insulators have excellent thermoelectric properties and can be used as potentially highly-efficient thermoelectric materials. For example, Ma et al.[27] studied the thermoelectric transport properties of the three-dimensional topological insulator thin film and found that thermoelectric coefficients exhibit rich behaviors. Zhang et al.[28] found that the thermoelectric effect of the topological insulator thin films is mainly determined by the bulk states. Yang et al.[12] studied the thermoelectric properties of the surface states in three-dimensional topological insulator nanowires and found that thermoelectric coefficient is strongly dependent on the gate voltage and the magnetic fields. Chen et al.[29] found that the optimal ZT in the topological phase transition region of the topological insulator. These studies have provided a new idea for performance optimization of thermoelectric materials.

The quantum spin-Hall effect (QSH) was first theoretically predicted to exist in Graphene and two-dimensional semiconductor systems[30,31]. QSH state is a completely new matter state which is different from the quantum Hall state, and its implementation does not require an external magnetic field. QSH state has helical edge states, preserves time-reversal invariance. In the QSH system, the bulk state is insulated with an independent energy gap between the conduction and valence band, and the gapless edge states are topologically protected from impurities, which is actually the two-dimensional topological insulators[32–34]. Recently, based on the existence of quantum point contacts and quantum dots, several devices of heat engines and refrigerators have been proposed by using nature of the quantum Hall edge states. Such as: Sánchez et al.[35] studies the thermoelectric properties of the three-terminal quantum Hall conductor and determines the contribution of the thermoelectric response dependent on the chirality of the carrier motion rather than spatial asymmetry. Roura-Bas et al.[36] investigated the thermoelectric response of a quantum dot embedded in a constriction of a quantum Hall bar. By applying the gate voltage and the magnetic field on the quantum dot, different thermoelectric working modes can be induced in the device. Takahashi et al.[37] studied the thermoelectric properties of two-dimensional quantum spin Hall systems and found that edge-state transport is dominant in low-temperature thermoelectric transport. Roura-Bas et al.[38] studied the thermoelectric response of a setup containing a pair of helical edge states and found that different thermoelectric operational modes can be induced by using the gate voltage and magnetic field. Gresta et al.[39] studied the thermoelectric properties of a Kramers pair of helical edge states of the quantum spin Hall effect coupled to a nanomagnet and found that this device can achieve high-performance thermoelectric transport in the linear response regime. However, since the temperature difference is less than the temperature, the efficiency η remains low in the linear region, even if ZT can be very large. In terms of practical usage, devices need to be run at finite power output, where the linearization may not work anymore. A deeper study of the nonlinear thermoelectric transport is needed to accurately assess the thermoelectric properties of the device. Based on the work of Gresta et al.[39], we studied the linear and nonlinear thermoelectric transport of helical edge states of the quantum spin Hall effect coupled to a nanomagnet by using the device shown in Fig. 1, and analyzed the impact of the length of the two nanomagnets and the relative tilt angle of component of the magnetization perpendicular on the thermoelectric coefficient. In contrast to the work of Gresta et al.[39], we tended to focus on the nonlinear thermoelectric transport properties in a quantum spin Hall insulator coupled to nanomagnets, and obtained the temperature difference of achieving optimal equivalent figure of merit ZT_M and power-generation efficiency η. Finally, it has been further proved that this setup can be used as an efficient and useful thermoelectric device, and it is very attractive and promising for the application of the thermoelectricity.

Results

Thermoelectric properties in linear response. Firstly, the transmission function $T(E)$ was calculated with Eq. (4), and the change of $T(E)$ is showed in Fig. 2. In the calculation, the length of the two nanomagnets of equal size is taken as l=L/L_0= 10, 4, 2, 1 respectively. The relative tilt angle of magnetic moment perpendicular component orientation of one of the nanomagnet is $\phi_1 = 0$, the other is $\phi_2 = \phi$. As can be seen from Fig. 2, when the $l = 10$, a gap opens in the spectrum of the helical edges. The transmission function tends to a step function, and there is no resonance in the opening of the gap. When the length of the magnetic domains is taken $l = 4$, 2 and 1, there is a resonance in the magnetic domains. The resonance position of different relative tilt ϕ is different. The width of the resonance decreases with l increases. These results are in full agreement with Ref.[39],

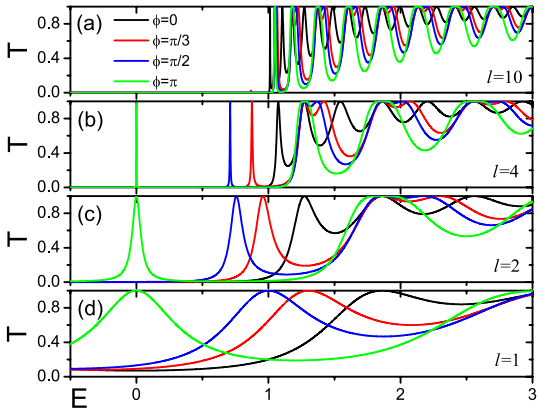

Figure 2. Transmission function for two magnetic domains of equal size (l=L/L_0= 10, 4, 2, 1), with the perpendicular component of the magnetic moments oriented with a relative tilt ϕ. Energies ($E = \varepsilon/\varepsilon_\perp$) are expressed in units of $\varepsilon_\perp = Jm_\perp$, and lengths are expressed in units of $L_0 = \varepsilon_\perp/\hbar v_F$.

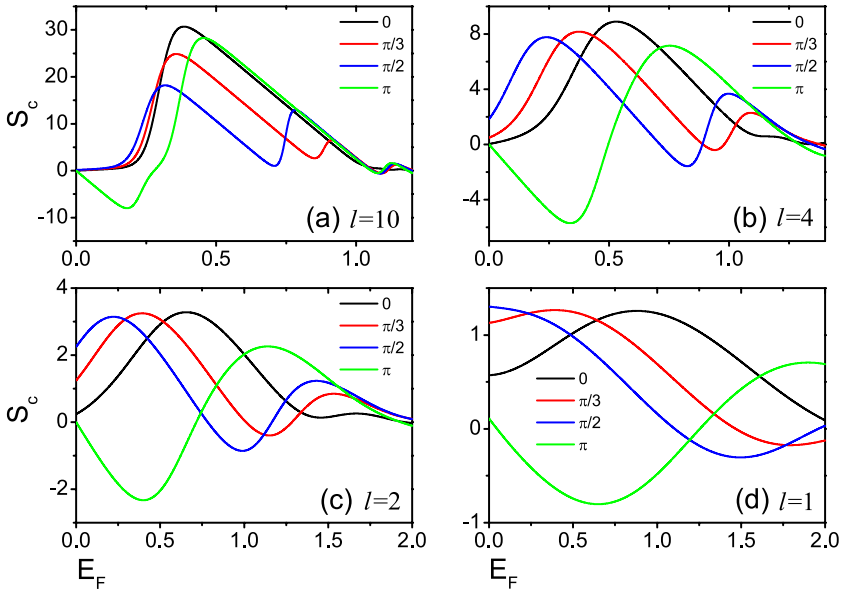

Figure 3. The Seebeck coefficients S_c as functions of Fermi energy E_F for several relative tilt ϕ with temperature $\mathcal{T}/\mathcal{T}_0 = 0.02$ in (**a**), and $\mathcal{T}/\mathcal{T}_0 = 0.05$ in (**b**), and $\mathcal{T}/\mathcal{T}_0 = 0.1$ in (**c**) and $\mathcal{T}/\mathcal{T}_0 = 0.05$ in (**d**). Two magnetic domains of equal size l= 10, 4, 2, 1. The temperatures are expressed in units of $\mathcal{T}_0 = \varepsilon_\perp/k_B$.

but it is different that the current results of $l = 4$ and $l = 2$ calculations are fully consistent with the trends in $l = 10$ and $l = 4$ in Ref.[39] respectively.

Next, we focus on the linear thermoelectric properties of the devices of Fig. 1. Figures 3 and 4 show the Seebeck coefficient S_c and the thermoelectric figure of merit ZT versus the Fermi energy E_F for several relative tilt ϕ. Two magnetic domains of equal size l are taken 10, 4, 2 and 1 respectively. S_c and ZT exhibit a series of peaks at low temperatures. When $l = 4, 2, 1$, the existence of resonance needed to be noticed in Fig. 2, while the resonance width increases gradually with the decrease of l, and the corresponding thermoelectric coefficients (S_c and ZT) decrease gradually in Figs. 3 and 4. For $l = 10$, no resonance is present in Fig. 2, but both S_c and ZT is very large in Figs. 3 and 4. The value of ZT at the highest peak exceeds 800 at low temperature. This is determined by the open gap in the spectrum of the helical edges. To obtain a larger ZT value, it is necessary to have high conductivity G to reduce electron heating, high Seebeck coefficient S_c to ensure the output voltage and low thermal conductivity κ to maintain large temperature difference. Generally speaking, these three parameters are related to the energy band structure of the material. When the system has an energy gap and the Fermi energy is near the conduction band edge, it will lead to a small thermal conductivity and a large Seebeck coefficient. As a result, ZT has a large value[12,40–42]. This suggests that the opening of a gap in the spectrum of the helical edges is very beneficial to the thermoelectric transport of the device, and similar conclusions are shown in Ref.[39]. Furthermore, it is seen from Fig. 4 that the ZT value of $\phi = \pi$ for l=10, 4 is much greater than other values of ϕ.

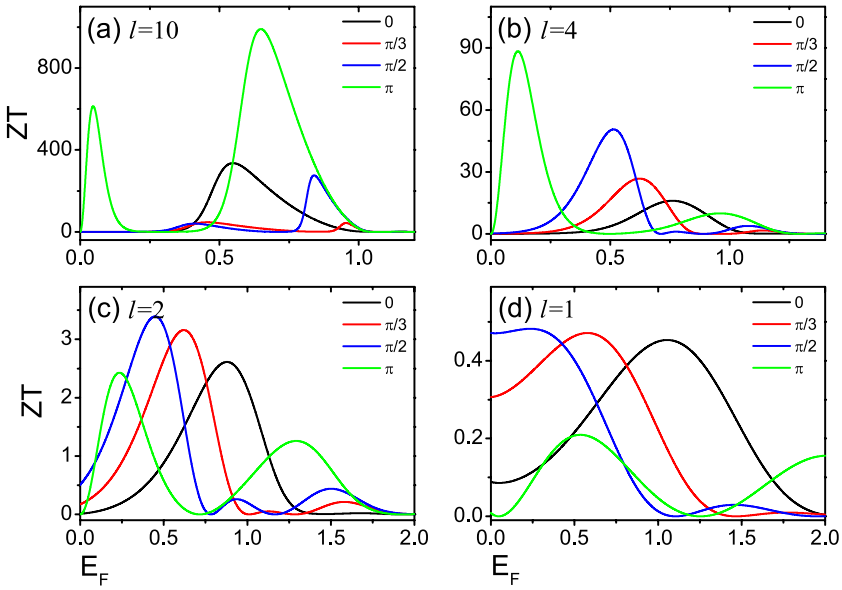

Figure 4. The thermoelectric figure of merit ZT as functions of Fermi energy E_F for several relative tilt ϕ with temperature $\mathcal{T}/\mathcal{T}_0 = 0.02$ in (**a**), and $\mathcal{T}/\mathcal{T}_0 = 0.05$ in (**b**), and $\mathcal{T}/\mathcal{T}_0 = 0.1$ in (**c**) and $\mathcal{T}/\mathcal{T}_0 = 0.05$ in (**d**). The other unmentioned parameters are the same as in Fig. 3.

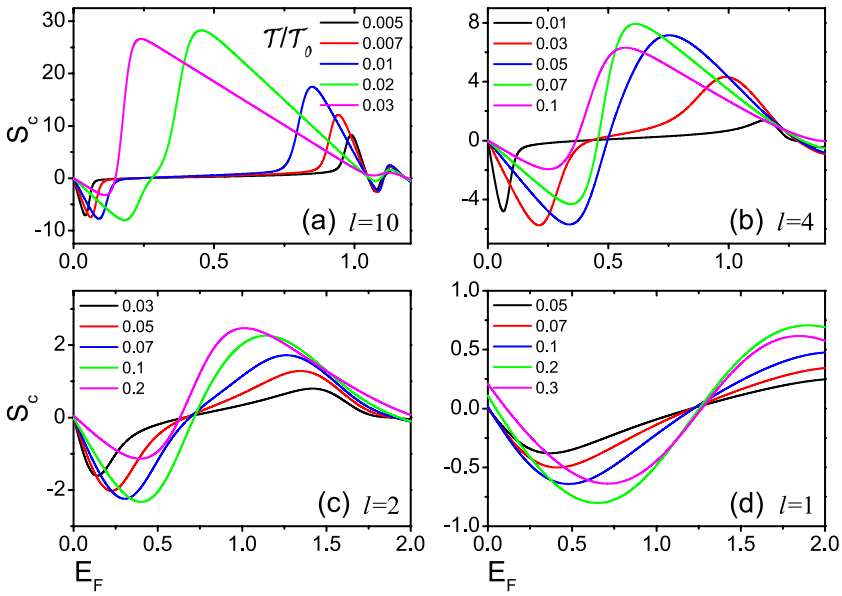

Figure 5. The Seebeck coefficients S_c as functions of Fermi energy E_F for different temperatures $\mathcal{T}/\mathcal{T}_0$ with relative tilt $\phi = \pi$. The temperatures are expressed in units of $\mathcal{T}_0 = \varepsilon_\perp/k_B$. Two magnetic domains of equal size $l = 10$ in (**a**), and $l = 4$ in (**b**), and $l = 2$ in (**c**) and $l = 1$ in (**d**).

This is because a large energy difference between the peaks is observed for the two nanomagnets with $\phi = \pi$, and the first peak after the closing of the gap leads to higher ZT peaks. For $l = 2$, 1, the ZT values are small, so the height of ZT peaks varies slightly for several relative tilt ϕ.

At last, we study how the temperature affects the thermoelectric transport in detail. When $\phi = \pi$, the values of S_c, and ZT are larger than those of other relative tilt ϕ (see Figs. 3, 4). So, Figs. 5 and 6 show the Seebeck coefficient S_c and the thermoelectric figure of merit ZT versus Fermi energy E_F at different temperatures with relative tilt $\phi = \pi$. For l=10, S_c display a large peak at low temperatures with $0 < E_F < 1$, with the corresponding ZT also has a large value (see Figs. 5a, 6a). This is because there is no resonance with $0 < E_F < 1$, and the open energy gap implies that the transmission function $T(E) = 0$. A large bias which is required to balance the thermal forces acting on the charge carriers has resulted in very large S_c, and ZT. For $l = 4$, 2 and 1, there is a resonance in the magnetic domains, and the width of the resonance decreases for increasing l. The first peak of resonance

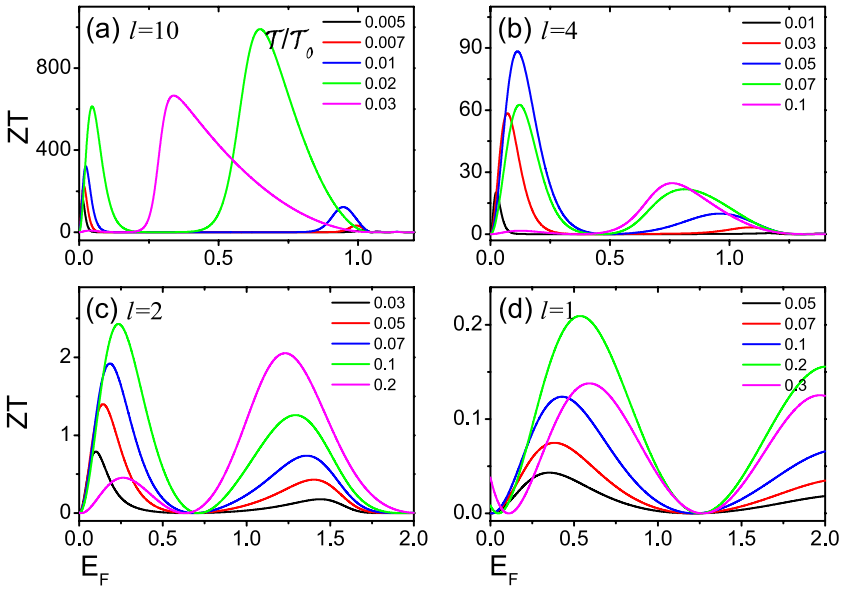

Figure 6. The thermoelectric figure of merit ZT as functions of Fermi energy E_F for different temperatures $\mathcal{T}/\mathcal{T}_0$ with relative tilt $\phi = \pi$. Two magnetic domains of equal size $l = 10$ in (**a**), and $l = 4$ in (**b**), and $l = 2$ in (**c**) and $l = 1$ in (**d**). The other unmentioned parameters are the same as in Fig. 5.

after the closing of the gap would generate a large thermoelectric coefficients (S_c, and ZT)[39]. For $E_F \sim k_B\mathcal{T}$, the resonance within the gap affects the thermoelectric response coefficients, and leads to larger ZT. ZT values is strongly associated with the width of the resonance[39]. For the higher temperatures, when the transport behavior is controlled by the Heaviside function[39], the thermoelectric coefficient ZT is affected by several peaks and the value of ZT decreases.

Thermoelectric properties in nonlinear regime. In this section, we will focus on studying the thermoelectric transport properties of this device in the nonlinear regime, computing the equivalent figure of merit ZT_M and the power-generation efficiency η. Unlike the linear case, in the nonlinear region, there will be a finite bias ΔV and a temperature gradient $\Delta\mathcal{T}$ between two leads of the device. In the calculation, we take the right lead temperature is the same as the background temperature $\mathcal{T}_R = \mathcal{T}$, so the left lead temperature is $\mathcal{T}_L = \mathcal{T} + \Delta\mathcal{T}$. In addition, we label the chemical potentials of the left and right leads as μ_L and μ_R, and $\mu_R > \mu_L$. In Eq. (7), we fixed μ_L to find the maximum power-generation efficiency η by changing μ_R and then using Eq. (8) to calculate the equivalent figure of merit ZT_M. Figure 7 shows the efficiency η and the equivalent figure of merit ZT_M as functions of the chemical potential μ_L for different temperature gradient $\Delta\mathcal{T}$ with two magnetic domains of equal size $l = 10$ and 4.

In order to illustrate the reliability and reasonableness of the present calculations, we first compared the equivalent figure of merit ZT_M calculated in the nonlinear region with the ZT calculated in the linear response. In Fig. 7c, the thick black lines represent ZT as functions of the Fermi energy E_F in the linear response and the red lines represent the equivalent figure of merit ZT_M of $\Delta\mathcal{T} = 0.0005$ for $l = 10$ in the nonlinear region. It can be seen that the ZT in the linear region is fully consistent with the ZT_M of $\Delta\mathcal{T} = 0.0005$ in the nonlinear region. For $l = 4$ (see Fig. 7d), we can also draw similar conclusions. This suggests that the nonlinear ZT_M regresses to the linear ZT when the nonlinear temperature difference $\Delta\mathcal{T} \to 0$. This indicates that the current calculation is completely reasonable and reliable.

Next, the thermoelectric properties in the nonlinear regime can be further explored. For $l = 10$, no resonance is present (see Fig. 2), but both S_c and ZT are very large in the linear case [see Figs. 3a, 4a]. Thus, we take the $l = 10$, the relative tilt $\phi = \pi$, and the background temperature $\mathcal{T} = 0.02$ in Fig. 7a,c. It is seen from the figure that as the increase of the temperature difference $\Delta\mathcal{T}$ from 0.0005 to 0.04, the equivalent figure of merit ZT_M decreases monotonically with the $\Delta\mathcal{T}$, while the power-generation efficiency η increases monotonically with $\Delta\mathcal{T}$. When the temperature difference $\Delta\mathcal{T} = 0.02$, the efficiency exceeds $\eta > 40\%$, and the equivalent figure of merit ZT_M also exceeds 200. Such a high equivalent figure of merit ZT_M and such a large power-generation efficiency η indicate that this devices have the necessary conditions to achieve high-performance thermoelectric power.

The equivalent figure of merit ZT_M for the nonlinear region l= 4 is much smaller than l= 10, which is also similar to the case in the linear region. In Fig. 7b,d, we take the $l = 4$, the relative tilt $\phi = \pi$, and the background temperature $\mathcal{T} = 0.05$. In the linear response, for $l = 4$, there is a resonance in the magnetic domains [see Fig. 2]. However, for the nonlinear thermoelectric transport, the equivalent figure of merit ZT_M is not monotonically dependent on $\Delta\mathcal{T}$, and ZT_M increases firstly and then decreases slightly as the temperature difference $\Delta\mathcal{T}$ increases from 0.0005 to 0.08. When the temperature difference $\Delta\mathcal{T}$=0.01, ZT_M is maximum, $ZT_M \approx 95$. The power-generation efficiency η increases with the increase of $\Delta\mathcal{T}$. Although the Carnot power-generation efficiency exceeds 30%, the equivalent figure of merit ZT_M is extremely reduced when the temperature difference

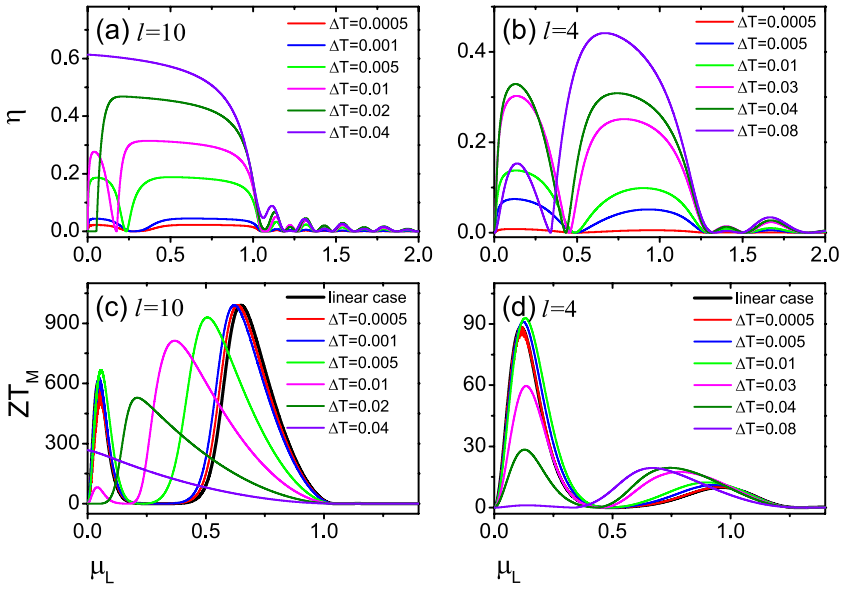

Figure 7. The efficiency η and the equivalent figure of merit ZT_M as a function of the chemical potential μ_L for different temperature gradient $\Delta\mathcal{T}$, with the background temperature $\mathcal{T}_R = \mathcal{T} = 0.02$ in (**a,c**); $\mathcal{T}_R = \mathcal{T} = 0.05$ in (**b,d**). Two magnetic domains of equal size $l = 10$ with $\phi = \pi$ in (**a,c**); $l = 4$ with $\phi = \pi$ in (**b,d**). The thick black lines in (**c,d**) are ZT in the linear regime. The other unmentioned parameters are the same as in Fig. 3.

$\Delta\mathcal{T} = 0.04$ and 0.08. Overall, making the efficiency $\eta > 20\%$ and the equivalent figure of merit $ZT_M > 10$, we believe that the temperature has difference $\Delta\mathcal{T} = 0.03$ or so.

Conclusion

In summary, the thermoelectric transport properties of helical edge states of the two-terminal nanoribbon of quantum spin Hall insulators coupling double nanomagnets have been studied, and the Seebeck coefficients S_c and the thermoelectrical figure of merit ZT, the equivalent figure of merit ZT_M and the power-generation efficiency η for linear and nonlinear thermoelectric transport have been calculated. Because the previous paper[39] has confirmed that it is necessary to have the device for achieving high performance thermoelectric power. We further explored the effect of the length of the nanomagnet and the relative tilt angle of component of the magnetization perpendicular on the thermoelectric transport properties, obtained the temperature difference of achieving optimal equivalent figure of merit ZT_M and power-generation efficiency η. This setup (quantum spin Hall insulators coupling two nanomagnets) has a potential application as a thermoelectric device.

Methods

Hamiltonian and transmission function. The device coupling nanomagnet to the quantum spin Hall edge insulator is shown in Fig. 1, whose Hamiltonian can be represented as[39],

$$H = \int dx\, c^{\dagger}(x)[(-i\hbar v_F\partial_x)\hat{\boldsymbol{\sigma}}_z + J\mathbf{m}(x)\cdot\hat{\boldsymbol{\sigma}}]c(x), \tag{1}$$

where $c(x) = (c_{R,\uparrow}(x), c_{L,\downarrow}(x))^T$, and $\hat{\boldsymbol{\sigma}} = (\hat{\boldsymbol{\sigma}}_x, \hat{\boldsymbol{\sigma}}_y, \hat{\boldsymbol{\sigma}}_z)$ is the Pauli matrices. Here, the electrons with velocity v_F and $\uparrow$ ($\downarrow$) spin orientation move to the right (left). J is the magnetic exchange interaction between the magnetic moment of the nanomagnet and the electron spin. The nanomagnet is described by the spatial distribution of the magnetic moments within the segments of lengths $L_j = x_j - x_{j-1}$[39], so

$$\mathbf{m}(x) = \sum_{j=1}^{N} \zeta(x_j - x)\zeta(x - x_{j-1})\mathbf{m}_j, \tag{2}$$

where $\mathbf{m}_j = (m_{j\perp}\cos\phi_j, m_{j\perp}\sin\phi_j, m_{j\parallel})$ is a magnetic moment per unit length associated with the direction of spin-orb interaction in topological insulators, $m_{j\parallel}$ is a parallel component and $m_{j\perp}$ is a perpendicular component.

For the calculation of the transmission function, refer to Refs.[39,43], applying the evolution operator in space throughout the scattering region, $\hat{u}(x_N, x_0) = \Pi_{j=1}^{N}\hat{u}(x_j, x_{j-1})$. Therefore, the transmission function[39] can be expressed as $T(E) = \mid \mathbf{Det}[\hat{u}(x_N, x_0)]/u(x_N, x_0)_{1,1} \mid^2$, here

$$\begin{aligned}\hat{u}(x_j, x_{j-1}) =& e^{\left(i\frac{E_{j\parallel}}{\hbar v_F}L_j\right)} e^{(-i\xi_j\cdot\hat{\boldsymbol{\sigma}})} \\ =& e^{\left(i\frac{E_{j\parallel}}{\hbar v_F}L_j\right)} \left[\hat{\boldsymbol{\sigma}}_0 \cos\lambda_j - i\mathbf{n}_j\cdot\hat{\boldsymbol{\sigma}}\sin\lambda_j\right],\end{aligned} \tag{3}$$

where $\xi_j = (iE_{j\perp}\sin\phi_j, -iE_{j\perp}\cos\phi_j, E)L_j/(\hbar v_F)$, with $E_{\parallel,\perp} = Jm_{\parallel,\perp}$ and $\mathbf{n}_j = \frac{\xi_j}{\lambda_j}$.

In this paper, for two nanommagnets, the length is the same, while the orientation of the magnetic moment is different. So $N = 2$ in Eq. (2), $L_1 = L_2 = L$, $\phi_1 = 0$, $\phi_2 = \phi$ and $E_{\perp,1} = E_{\perp,2} = E_\perp$ in Eq. (3). The transmission function can be written as[39]

$$T(E) = \left\{\left[\cos^2\lambda + \frac{\sin^2\lambda}{r^2}\left(\cos\phi - \frac{E^2}{E_\perp^2}\right)\right]^2 + \left[-\frac{E}{E_\perp}\frac{\sin 2\lambda}{r} + \sin\phi\frac{\sin^2\lambda}{r^2}\right]^2\right\}^{-1}, \tag{4}$$

here, $\lambda = rl$ and $r = \sqrt{(\frac{E}{E_\perp})^2 - 1}$, where $l = \frac{L}{L_0}$ and $L_0 = \frac{\hbar v_F}{E_\perp}$.

Thermoelectric transport. In the linear response region, the electric and heat currents are expanded linearly in a small temperature difference $\delta\mathcal{T} = \mathcal{T}_L - \mathcal{T}_R$ and a small external bias voltage $\delta V = V_L - V_R$[14,16,17],

$$\begin{pmatrix} I_L \\ I_L^Q \end{pmatrix} = \begin{pmatrix} e^2\mathcal{D}_0 & -e\mathcal{D}_1 \\ -e\mathcal{D}_1 & \mathcal{D}_2 \end{pmatrix}\begin{pmatrix} \delta V \\ \delta\mathcal{T}/\mathcal{T} \end{pmatrix}. \tag{5}$$

In Eq. (5), the elements of the Onsager matrix is given by $\mathcal{D}_i = \frac{1}{h}\int dE\ (E - E_F)^i(-\frac{\partial f}{\partial E})T(E)$, where $i = 0, 1, 2$ and $f(E) = \left[e^{(E-E_F)/k_B\mathcal{T}} + 1\right]^{-1}$. The transmission function $T(E)$ can be obtained from Eq. (4).

Using Eq. (5), the linear electric conductance G, the Seebeck coefficients S_c, and the electric thermal conductance κ_{el} can be expressed as[14,17] $G = \lim_{\delta V\to 0}\frac{I_L}{\delta V}\Big|_{\delta\mathcal{T}=0} = e^2\mathcal{D}_0$, $S_c = -\lim_{\delta\mathcal{T}\to 0}\frac{\delta V}{\delta\mathcal{T}}\big|_{I_L=0} = -\frac{1}{e\mathcal{T}}\frac{\mathcal{D}_1}{\mathcal{D}_0}$ and $\kappa_{el} = -\lim_{\delta\mathcal{T}\to 0}\frac{I_L^Q}{\delta\mathcal{T}}\Big|_{I_L=0} = \frac{1}{\mathcal{T}}\frac{\mathcal{D}_0\mathcal{D}_2 - \mathcal{D}_1^2}{\mathcal{D}_0}$. We can also write the thermoelectric figure of merit $ZT = GS_c{}^2\mathcal{T}/\kappa_{el} = \frac{\mathcal{D}_1^2}{\mathcal{D}_0\mathcal{D}_2 - \mathcal{D}_1^2}$, straightforwardly. Here, the lattice thermal conductance κ_{ph} is ignored. This is because the lattice thermal conductivity is caused by the lattice vibration. At the low temperature, the lattice thermal conductance is overshadowed by the electronic thermal conductance.

In the nonlinear regime, the temperature difference $\delta\mathcal{T}$ and external bias voltage δV are finite. Here set the temperature difference $\Delta\mathcal{T} > 0$, the electric and heat currents can be written as[44–47]

$$\begin{aligned} I_L &= \frac{e}{h}\int dE\ T(E)[f_L(\mu_L, \mathcal{T}_L; E) - f_R(\mu_R, \mathcal{T}_R; E)], \\ I_\alpha^Q &= \frac{1}{h}\int dE\ (E - \mu_\alpha)T(E)[f_L(\mu_L, \mathcal{T}_L; E) - f_R(\mu_R, \mathcal{T}_R; E)], \end{aligned} \tag{6}$$

where $f_\alpha(\mu_\alpha, \mathcal{T}_\alpha; E) = \left[e^{(E-\mu_\alpha)/k_B\mathcal{T}_\alpha} + 1\right]^{-1}$ is the Fermi distribution function, μ_α is the chemical potential of α-lead, with $\alpha = L, R$.

In this paper, the device can be seen as a power generator, so its power output P and efficiency of the power generator η can be expressed as[44–47]

$$\begin{aligned} P &= -I_C\Delta V = \frac{1}{h}(\mu_R - \mu_L)\int dE\ T(E)[f_L(\mu_L, \mathcal{T}_L; E) - f_R(\mu_R, \mathcal{T}_R; E)], \\ \eta &= \frac{P}{I_L^Q} = \frac{(\mu_R - \mu_L)\int dE\ T(E)[f_L(\mu_L, \mathcal{T}_L; E) - f_R(\mu_R, \mathcal{T}_R; E)}{\int dE\ (E - \mu_L)T(E)[f_L(\mu_L, \mathcal{T}_L; E) - f_R(\mu_R, \mathcal{T}_R; E)]}. \end{aligned} \tag{7}$$

In this power generator, we set $\mu_R > \mu_L$ satisfying $P > 0$. In the calculation, the temperatures $\mathcal{T}_{L/R}$ and chemical potential μ_L is fixed, the μ_R is changed, the maximum power-generation efficiency η is given. Furthermore, considering the $\eta = \frac{\mathcal{T}_L - \mathcal{T}_R}{\mathcal{T}_L}\cdot\frac{\sqrt{1+ZT_M}-1}{\sqrt{1+ZT_M}+\frac{\mathcal{T}_R}{\mathcal{T}_L}}$[1,14], the equivalent thermoelectric figure of merit ZT_M is derived in terms of η,

$$ZT_M = \left[\frac{(\mathcal{T}_L - \mathcal{T}_R) + \eta\mathcal{T}_R}{(\mathcal{T}_L - \mathcal{T}_R) - \eta\mathcal{T}_L}\right]^2 - 1. \tag{8}$$

Further, we take $\mathcal{T}_R = \mathcal{T}$ and $\mathcal{T}_L = \mathcal{T} + \Delta\mathcal{T}$, $\mathcal{T}$ is the background temperature. Therefore, the maximum power-generation efficiency and the equivalent figure of merit can be written as[14]

$$\eta = \frac{\Delta\mathcal{T}}{\mathcal{T}+\Delta\mathcal{T}}\frac{\sqrt{1+ZT_M}-1}{\sqrt{1+ZT_M}+\mathcal{T}/(\mathcal{T}+\Delta\mathcal{T})},$$
$$ZT_M = \left[\frac{\Delta\mathcal{T}+\eta\mathcal{T}}{\Delta\mathcal{T}-\eta(\mathcal{T}+\Delta\mathcal{T})}\right]^2 - 1. \quad (9)$$

Data availability

The datasets used during the current study available from the corresponding author on request. Correspondence and requests for materials should be addressed to R.W.

Received: 17 March 2022; Accepted: 4 July 2022
Published online: 14 July 2022

References

1. He, J. & Tritt, T. M. Advances in thermoelectric materials research looking back and moving forward. *Science* **357**, eaak9997 (2017).
2. Tritt, T. M. Thermoelectric phenomena, materials, and applications. *Annu. Rev. Condens. Matter Phys.* **41**, 433 (2011).
3. Snyder, G. J. & Toberer, E. S. Complex thermoelectric materials. *Nat. Mater.* **7**, 105 (2008).
4. Majumdar, A. Thermoelectricity in semiconductor nanostructures. *Science* **303**, 777 (2004).
5. Shakouri, A. Recent developments in semiconductor thermoelectric physics and materials. *Annu. Rev. Condens. Matter Phys.* **41**, 399 (2011).
6. Callen, H. B. The application of Onsager's reciprocal relations to thermoelectric, thermomagnetic, and galvanomagnetic effects. *Phys. Rev.* **73**, 1349 (1948).
7. Callen, H. B. A note on the adiabatic thermomagnetic effects. *Phys. Rev.* **85**, 16 (1952).
8. Xu, Y. Thermoelectric effects and topological insulators. *Chin. Phys. B* **25**, 117309 (2016).
9. Xing, Y., Sun, Q. F. & Wang, J. Nernst and Seebeck effects in a graphene nanoribbon. *Phys. Rev. B* **80**, 235411 (2009).
10. Wei, M. M. *et al.* Magnetothermoelectric transport properties of multiterminal graphene nanoribbons. *Phys. Rev. B* **93**, 245432 (2016).
11. Zhang, Y., Song, J. T. & Li, Y. X. Nernst and Seebeck effects in HgTe/CdTe topological insulator. *J. Appl. Phys.* **117**, 124301 (2015).
12. Yang, N. X., Zhou, Y. F., Lv, P. & Sun, Q. F. Gate voltage controlled thermoelectric figure of merit in three-dimensional topological insulator nanowires. *Phys. Rev. B* **97**, 235435 (2018).
13. Bulman, G. E., Siivola, E., Shen, B. & Venkatasubramanian, R. Large external ΔT and cooling power densities in thin-film Bi2Te3-superlattice thermoelectric cooling devices. *Appl. Phys. Lett.* **89**, 122117 (2006).
14. Yang, N. X., Yan, Q. & Sun, Q. F. Linear and nonlinear thermoelectric transport in a magnetic topological insulator nanoribbon with a domain wall. *Phys. Rev. B* **102**, 245412 (2020).
15. Xu, N., Xu, Y. & Zhu, J. Topological insulators for thermoelectrics. *NPJ Quant. Mater.* **2**, 51 (2017).
16. Liu, J., Sun, Q. F. & Xie, X. C. Enhancement of the thermoelectric figure of merit in a quantum dot due to the Coulomb blockade effect. *Phys. Rev. B* **81**, 245323 (2010).
17. Costi, T. A. & Zlatic, V. Thermoelectric transport through strongly correlated quantum dots. *Phys. Rev. B* **81**, 235127 (2010).
18. Müchler, L., Casper, F., Yan, B., Chadov, S. & Felser, C. Topological insulators and thermoelectric materials. *Phys. Status Solidi RRL* **7**, 91 (2013).
19. Kolenda, S., Machon, P., Beckmann, D. & Belzig, W. Nonlinear thermoelectric effects in high-field superconductor-ferromagnet tunnel junctions. *Beilstein J. Nanotechnol.* **7**, 1579 (2016).
20. López, R. & Sánchez, D. Nonlinear heat transport in mesoscopic conductors: Rectification, Peltier effect, and Wiedemann-Franz law. *Phys. Rev. B* **88**, 045129 (2013).
21. Leijinse, M., Ewgewijs, M. R. & Flensberg, K. Nonlinear thermoelectric properties of molecular junctions with vibrational coupling. *Phys. Rev. B* **82**, 045412 (2010).
22. Ruokola, T., Ojanen, T. & Jauho, A. P. Thermal rectification in nonlinear quantum circuits. *Phys. Rev. B* **79**, 144306 (2009).
23. Kuo, D. M. & David, M. T. Thermoelectric and thermal rectification properties of quantum dot junctions. *Phys. Rev. B* **81**, 205321 (2010).
24. Whitney, R. S. Thermodynamic and quantum bounds on nonlinear dc thermoelectric transport. *Phys. Rev. B* **87**, 115404 (2013).
25. Hasan, M. Z. & Kane, C. L. Colloquium: Topological insulators. *Rev. Mod. Phys.* **82**, 3045 (2010).
26. Qi, X. L. & Zhang, S. C. Topological insulators and superconductors. *Rev. Mod. Phys.* **83**, 1057 (2011).
27. Ma, R., Sheng, L., Liu, M. & Sheng, D. N. Thermoelectric transport in thin films of three-dimensional topological insulators. *Phys. Rev. B* **87**, 115304 (2013).
28. Zhang, J. *et al.* Disentangling the magnetoelectric and thermoelectric transport in topological insulator thin films. *Phys. Rev. B* **91**, 075431 (2015).
29. Chen, L. C. *et al.* Enhancement of thermoelectric performance across the topological phase transition in dense lead selenide. *Nat. Mater.* **18**, 1321 (2019).
30. Kane, C. L. & Mele, E. J. Quantum Spin Hall effect in graphene. *Phys. Rev. Lett.* **95**, 226801 (2005).
31. Bernevig, B. A. & Zhang, S. C. Quantum Spin Hall effect. *Phys. Rev. Lett.* **96**, 106802 (2006).
32. Bernevig, B. A., Hughes, T. L. & Zhang, S. C. Quantum Spin Hall effect and topological phase transition in HgTe quantum wells. *Science* **314**, 1757 (2006).
33. König, M. *et al.* Quantum Spin Hall insulator state in HgTe quantum wells. *Science* **318**, 5851 (2007).
34. Qi, X. L. & Zhang, S. C. The quantum Spin Hall effect and topological insulators. *Phys. Today* **63**, 33 (2010).
35. Sánchez, R., Sothmann, B. & Jordan, A. N. Chiral thermoelectrics with quantum Hall Edge states. *Phys. Rev. Lett.* **114**, 146801 (2015).
36. Roura-Bas, P., Arrachea, L. & Fradkin, E. Enhanced thermoelectric response in the fractional quantum Hall effect. *Phys. Rev. B* **97**, 081104(R) (2018).
37. Takahashi, R. & Murakami, S. Thermoelectric transport in perfectly conducting channels in quantum spin Hall systems. *Phys. Rev. B* **81**, 161302(R) (2010).
38. Roura-Bas, P., Arrachea, L. & Fradkin, E. Helical spin thermoelectrics controlled by a side-coupled magnetic quantum dot in the quantum spin Hall state. *Phys. Rev. B* **98**, 195429 (2018).
39. Gresta, D., Real, M. & Arrachea, L. Optimal thermoelectricity with quantum Spin Hall edge states. *Phys. Rev. Lett.* **123**, 186801 (2019).
40. Zlatić, V. & Freericks, J. K. Strongly enhanced thermal transport in a lightly doped mott insulator at low temperature. *Phys. Rev. Lett.* **109**, 266601 (2012).

41. Masood, K. B., Kumar, P. & Singh, R. A. Odyssey of thermoelectric materials: Foundation of the complex structure. *J. Phys. Commun.* **2**, 062001 (2018).
42. Ding, G., Gao, G. & Yao, K. High-efficient thermoelectric materials: The case of orthorhombic IV–VI compounds. *Sci. Rep.* **5**, 9567 (2015).
43. Bustos-Marun, R., Refael, G. & Von Oppen, F. Adiabatic quantum motors. *Phys. Rev. Lett.* **111**, 060802 (2013).
44. Hershfield, S., Muttalib, K. A. & Nartowt, B. J. Nonlinear thermoelectric transport: A class of nanodevices for high efficiency and large power output. *Phys. Rev. B* **88**, 085426 (2013).
45. Karbaschi, H., Lovén, J., Courteaut, K., Wacker, A. & Leijnse, M. Nonlinear thermoelectric efficiency of superlattice-structured nanowires. *Phys. Rev. B* **94**, 115414 (2016).
46. Gómez-Silva, G., Orellana, P. A. & Anda, E. V. Enhancement of the thermoelectric efficiency in a T-shaped quantum dot system in the linear and nonlinear regimes. *J. Appl. Phys.* **123**, 085706 (2018).
47. Bevilacqua, G., Grosso, G., Menichetti, G. & Pastori Parravicini, G. Thermoelectric efficiency of nanoscale devices in the linear regime. *Phys. Rev. B* **94**, 245419 (2016).

Acknowledgements

This work was supported by the Scientific Research Project of Shihezi University (Grant No. ZZZC202031B), NSF-China (Grants Nos. 12164038 and 62104162).

Author contributions

R.W. performed the research and calculations. R.W., H.L., C.-Y.S., G.-H.T. and N.-X.Y. discussed the results and wrote this paper together. R.W. supervised the project.

Competing interests

The authors declare no competing interests.

Additional information

Correspondence and requests for materials should be addressed to R.W.

Reprints and permissions information is available at www.nature.com/reprints.

Publisher's note Springer Nature remains neutral with regard to jurisdictional claims in published maps and institutional affiliations.